Effects of Plasma Processing Parameters on the Surface Reactivity of OH($X^2\Pi$) in Tetraethoxysilane/O_2 Plasmas during Deposition of SiO_2

K. H. A. Bogart,[†] J. P. Cushing,[‡] and Ellen R. Fisher*

Department of Chemistry, Colorado State University, Fort Collins, Colorado 80523-1872

Received: May 14, 1997; In Final Form: July 18, 1997[⊗]

The OH($X^2\Pi$) radical in a 20:80 tetraethoxysilane (TEOS)/O_2 plasmas has been characterized during deposition of SiO_2 using the imaging of radicals interacting with surfaces (IRIS) method. The reactivity of OH at the surface of a growing SiO_2 film has been determined as a function of the applied radio-frequency (rf) plasma power (P) and the substrate temperature (T_S). The reactivity (R) of OH during deposition of SiO_2 on a 300 K Si substrate is 0.41 ± 0.04. R decreases as substrate temperature increases but is unaffected by increasing rf power. Translational and rotational temperatures (Θ_T and Θ_R, respectively) of the OH radical are also determined. For a 20:80 TEOS/O_2 plasma ($P = 85$ W), $\Theta_T = 912 \pm 20$ K and $\Theta_R = 450 \pm 20$ K. Θ_T is significantly higher than Θ_R and increases with increasing rf power. Using isotopically labeled $^{18}O_2$ as a precursor, the source of the oxygen in OH is identified as the O_2 gas, not oxygen from the ethoxy groups on TEOS. With these data, the role of OH in deposition of SiO_2 from TEOS-based plasmas and the effects of plasma deposition parameters on film formation are discussed.

I. Introduction

Plasma-based processes such as plasma-enhanced chemical vapor deposition (PECVD) are indispensable for surface modification and deposition or etching of thin film materials.[1,2] Tetraethoxysilane (TEOS)-based plasmas are used extensively in the microelectronics industry to deposit silicon dioxide (SiO_2) for dielectric gate oxides in integrated circuits.[1−4] PECVD using TEOS with an oxidant yields nearly stoichiometric SiO_2 with conformal step coverage superior to films deposited from silane (SiH_4)-based plasmas.[1,3−7] Furthermore, TEOS is preferred over conventional silane sources because of its ease of use, chemical stability, and purity.[1,3,8]

Despite extensive industrial use, the mechanism for SiO_2 formation from TEOS/oxidant plasmas is not well understood. A review of recent literature suggests TEOS molecules are fragmented by plasma activation into di- or triethoxysilane molecules which are adsorbed onto the growing film surface.[1,7,9−12] The role of the added oxidant precursor gas is to oxidatively remove organic substituents from both gas-phase and adsorbed TEOS fragments, producing high-quality SiO_2.[1,8−12] This process can result in a high concentration of undesirable silanol (SiOH) species which disrupt the SiO_2 tetrahedral network. Empirical deposition studies have shown optimization of deposition parameters [applied rf power (P), oxidant concentration, or substrate temperature (T_S)] can reduce or eliminate silanols in these films.[7−11,13] Very little work has been done, however, to identify the specific plasma species and reactions responsible for film deposition. Investigation of the deposition process on a molecular level is needed to provide insight into the individual contributions of plasma species.

Characterization of gas-phase plasma species as well as molecules generated at a substrate surface during plasma modification can be achieved with the imaging of radicals interacting with surfaces (IRIS) method.[14,15] This method combines molecular beam and plasma technologies with spatially resolved laser-induced fluorescence (LIF) to measure radical surface reactivities (R) during plasma processing of a substrate. Reactivity measurements can be made under different plasma processing conditions by varying parameters such as P or T_S. The rotational temperature (Θ_R) for the molecule of interest is determined by analyzing the reactivity data as a function of both radical rotational state and T_S.[16,17] Using a state-of-the-art intensified charge coupled device (ICCD), the translational temperature (Θ_T) is measured by utilizing the temporal gating on the 2-D detector.[18] Further information on the mechanism for radical formation can be deduced through the use of isotopically labeled precursor gases.

To date, the IRIS method has been used to investigate five different radical species[14−19] in several plasma systems.[20,21] The OH radical, which is found in many chemical processes (i.e., combustion[22,23] and atmospheric reactions[24]), has been extensively studied with this technique.[14,16,19,20] OH is the only radical studied to date by the IRIS method that exhibits intermediate reactivity. Buss and co-workers found $R = 0.57 \pm 0.05$ for OH in a 100% H_2O plasma incident on a 300 K oxidized silicon nitride substrate, decreasing to zero at $T_S \geq 500$ K.[16] In this study, the OH radicals were characterized by very similar translational and rotational temperatures, $\Theta_T = 300 \pm 50$ and $\Theta_R = 340 \pm 20$ K. From these data, the authors suggested the OH radical is involved in an exchange mechanism with silanol groups present on the oxidized substrate surface. The water plasma, however, does not significantly etch the substrate or deposit a film. We have also measured the reactivity of OH in this system, $R = 0.55 \pm 0.05$,[14] using our third generation IRIS apparatus. The moderate reactivity of OH is intriguing, deserving of further study in different plasma processing systems.

An earlier communication from our laboratories reported a surface reactivity of 0.40 ± 0.10 for OH in a 20:80 TEOS/O_2 plasma ($P = 85$ W) while depositing SiO_2 on a 300 K silicon substrate.[19] Here, we expand our characterization of OH in TEOS-based plasmas to include reactivity measurements as a function of P and T_S. We also determine Θ_T and Θ_R for OH and the effect of P on OH radical energies. This more complete characterization of OH radicals in both the gas phase and at

[†] Present address: Bell Laboratories, Lucent Technologies, Murry Hill, NJ 07974.
[‡] Stanford Research Systems, Sunnyvale, CA 94089.
* To whom correspondence should be addressed.
[⊗] Abstract published in *Advance ACS Abstracts,* November 1, 1997.

S1089-5647(97)01596-4 CCC: $14.00

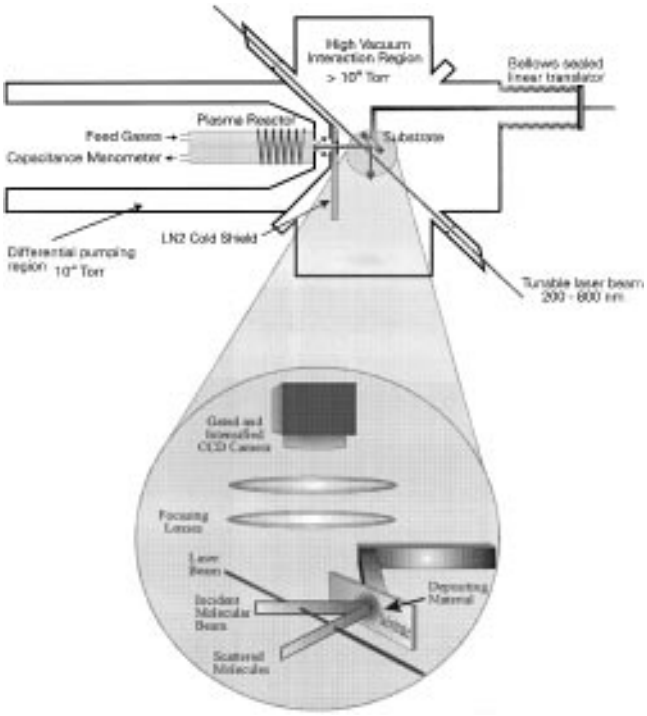

Figure 1. Schematic of IRIS apparatus showing expanded interaction region. The ICCD camera is located perpendicular to the plane of intersection of the laser beam and the molecular beam. Specular scattering is shown for clarity.

the surface of a depositing SiO_2 film provides elucidation of the chemical mechanisms involved in TEOS-based PECVD systems.

II. Experimental Methods

A. IRIS Apparatus. The IRIS apparatus, Figure 1, has been described in detail elsewhere.[14] A brief description is given here, concentrating on those aspects relevant to the present study. In a typical IRIS experiment, precursor gases enter a tubular glass chamber, rf power is applied, and a plasma is produced. Expansion into the vacuum chamber generates a near effusive molecular beam containing virtually all of the species in the plasma, including the species of interest. A tunable laser beam intersects the molecular beam at 45° and excites the chosen radical. Spatially resolved LIF signals are collected by an electronically gated, intensified charge-coupled device (ICCD). A substrate is rotated into the path of the molecular beam, and LIF signals are again collected. These data include LIF from molecules in the molecular beam as well as molecules scattering off the substrate surface. Differences between spatial distributions with the surface in and out of the molecular beam are used to determine the surface reactivity of the radical.

For the results presented here, the source of the molecular beam is a plasma produced from a mixture of TEOS (Schumacher Extrema, 99.99997%) and O_2 (General Air, 99.993%) or $^{18}O_2$ (Isotech 99%). The ratio of starting materials is defined using their partial pressures. TEOS vapor (10 mTorr) is sampled through the outlet valve of a stainless steel tank heated to 48 ± 1 °C, and its pressure is controlled by a bellows-sealed metering valve. Gas lines between the tank and the plasma chamber are heated (50−65 °C) to prevent condensation. O_2 gas flow (40 ± 5 mTorr) is controlled by an MKS mass flow controller. The two gases enter the plasma reactor in separate ports such that mixing occurs only in the plasma chamber. Total pressure in the source (50 ± 5 mTorr) is measured by an MKS capacitance manometer, which is insensitive to gas composition. The plasma is produced by the inductive coupling of 13.56 MHz rf power (22−115 W applied) and is tuned by a variable capacitor rf matching network.

The molecular beam is formed as the plasma diffuses from the plasma chamber into a differential region (base pressure = 1×10^{-7} Torr) and then into the main chamber (base pressure = 1×10^{-7} Torr). When the reactant gases are flowing, the pressures in the differential chamber and the main chamber rise to 1×10^{-4} and 2×10^{-5} Torr, respectively. The molecular beam is defined and collimated by two slits (1.0 and 1.25 mm wide, 19 mm high), located 38 and 50 mm, respectively, from the orifice of the plasma tube. This slit configuration was used for all experiments. The defining slit is cooled to liquid nitrogen temperatures by a cold shield to minimize desorption of molecules from the slit surfaces. The cold shield is a 100 × 150 × 5 mm copper block with 0.635 mm o.d. copper tubing surrounding a 13 × 25 mm slot. It is attached to the main chamber side of the differential wall, and the defining slit is mounted directly onto the cold shield, centered about the slot. The temperature is monitored by a K-type thermocouple attached directly to the copper block. The collimating slit is held in place by two aluminum straps also mounted on the cold shield and is located 12 mm from the defining slit.

The substrate is a 10 × 40 mm p-type silicon (100) wafer with ∼50 Å native oxide, single polished side facing the molecular beam. The wafer is mounted on a heatable substrate holder[14] and can be translated along the axis of the molecular beam. In these experiments, the substrate was located either 3 or 5 mm from the laser. The substrate is resistively heated (300−550 K) using a Kepco ATE 6-25M power supply (6 V, 25 A), and temperature is controlled by an Omega CN9000A temperature controller using a K-type thermocouple. Upon completion of an experiment, the substrate is removed from the IRIS apparatus, and the deposited film is analyzed by a Nicolet Magna 760 FTIR.

OH radicals are excited by laser light centered at 308 nm (∼500−1500 μJ/pulse) from a frequency-doubled excimer-pumped (XeCl, 100 mJ, 17 ns, 40 or 100 Hz) dye laser system with Rhodamine B (610). The resulting LIF signals are collected and focused onto the ICCD by two 50 mm fused silica lens ($f = 300$ mm and $f = 75$ mm). The optics demagnify the image so that the 12.9 mm long array views a region 55 mm long, making it possible to spatially resolve molecules in *both* the incident molecular beam and scattered from the surface simultaneously. The total area imaged by the ICCD is 1980 mm^2. A U340 band-pass filter is placed between the ICCD and the vacuum chamber to reduce spurious signals from continuous plasma emission and scattered laser light.

The LIF signals are collected with the ICCD gated on approximately 1.3 μs after the excitation pulse to avoid interference from the laser.[25] A gate width of 1.0 μs is used to collect the fluorescence over the entire radiative lifetime of the OH $A^2\Sigma^+$ state (688 ± 7 ns).[26] LIF signals are integrated by the ICCD for 10 accumulations of 2000 laser pulses. Fluorescence data are collected in sets with the surface alternating in and out of the molecular beam path. Background images are taken with either the laser tuned to an off-resonance frequency or the laser blocked and are subtracted from each data image. Multiple sets of data are taken for each experiment. Pixels are binned (4 × 4) to increase signal-to-noise and reduce processing time. A one-dimensional representation of the data image is made by averaging 14 columns (5.42 mm) of pixels containing the LIF signal and plotting signal intensity as a function of distance along the laser path.

For velocity measurements used to determine Θ_T, the gate delay is stepped in 0.5 μs increments from 1.252 to 3.252 μs. LIF images taken at each gate delay are a function of time and distance the molecules travel after excitation. This has been discussed in detail previously.[18] In the present system, the ICCD pixels are not binned to increase resolution, and one-dimensional distributions for LIF intensity as a function of distance are created by averaging several rows of pixels. Since the laser intersects the molecular beam at a 45° angle, this distance is corrected by a factor of 1.414. Velocity measurements made in our laboratory for other radicals have utilized the optimal geometry by setting the laser, molecular beam, and ICCD detector orthogonal to each other.[18]

Fluorescence excitation spectra are obtained to determine both the identity of the fluorescing species and the rotational temperature of the molecular beam. Here, the dye laser is stepped in 0.002 nm increments (0.001 nm doubled) with a 25 s ICCD exposure per step from 306.250 to 307.250 nm. Total fluorescence is collected and plotted as a function of wavelength.

B. Numerical Simulations. *1. Reactivity.* To quantify the molecular reactivity for the LIF signals acquired, a numerical simulation based on the experimental geometry is required.[15] This model calculates the spatial distribution of the radical number density in the molecular beam at the interaction region as well as the radical number density along the laser for molecules scattering from the substrate surface. To properly describe the spatial distribution of molecules emanating from a surface, a specific scattering mechanism must be assumed. Our simulation allows for two possible mechanisms, either specular scattering or adsorption−desorption (cosine distribution about the surface normal). The calculated curve for scatter assumes all of the incident radicals leave the substrate surface. To determine the reactivity of a specific molecule, the fraction of radicals scattering from the surface, *S*, is adjusted to best fit the experimental data. The surface reactivity, *R* is defined as $1 - S$. The experimental scattering ratio, Δ_{exp}, is defined as the ratio of the peak height maximum for the LIF signal resulting from scattered molecules to the peak height maximum for the LIF signal due to molecules in the incident molecular beam.

In addition to the experimental geometry, the effects of the kinetic energy and rotational state of the molecules are also included in these calculations. Molecules with different velocities will absorb slightly different wavelengths of light due to the Doppler effect.[27] In our experiments, the laser line width (0.5 cm^{-1}) is narrow enough to detect the effect of molecular velocity. The Doppler effect arises in our experiments because the laser is tuned to the peak of a rotational line to maximize LIF signal from OH in the molecular beam. OH radicals scattering from the substrate surface have velocity components along the laser beam that differ from the velocity components of the molecular beam. Therefore, scattered OH radicals experience a Doppler shift in absorption frequency, and detectability of these molecules is not optimal. The result is a detectable shift in position (up to ± 1 mm) and relative intensity of the LIF signal peak maximum (up to 50%) for the scattered OH radicals. A more detailed discussion of this effect in IRIS experiments can be found elsewhere.[16,17]

The rotational state of the radical can also influence the apparent Δ and *S* obtained from our experiments and numerical simulations. If the incident OH molecules adsorb onto the surface, thermally equilibrate, and then desorb, the internal energy of the scattered molecules is defined by T_S. The fraction of molecules in a specific *J* state is described by simple Boltzmann statistics

$$f_J = \frac{(2J+1)\exp-\left[\frac{BJ(J+1)}{kT}\right]}{\sum_{J=1}^{\infty}(2J+1)\exp-\left[\frac{BJ(J+1)}{kT}\right]} \quad (1)$$

where *k* is Boltzmann's constant, *T* is temperature, and *B* is the rotational constant.[28] If $T_S \neq \Theta_R$, then the population of a particular *J* state will change upon equilibration with the substrate. This will result in an apparent change in Δ since the scattering ratio is proportional to the ratio of *J*-state populations.[28]

$$\Delta \propto f_J(T_S)/f_J(\Theta_R) \quad (2)$$

The numerical simulation allows input of specific *J* state and T_S values for the calculation of Δ, and thus *S*, correcting for differences in rotational state populations.

2. Velocity Distribution. The numerical simulation for reactivity described above requires knowledge of the velocity for the radicals of interest in the molecular beam. The velocity of the radicals is measured directly from the data by determining the distance the two-dimensional LIF signal moves across the ICCD image as the gate delay on the ICCD is increased. Distance moved per unit time gives a velocity (υ) which is related to translational temperature, Θ_T. The data are also modeled using Monte Carlo methods to simulate the velocity profile of molecules as a function of distance traveled between excitation and collection of fluorescence.[18] The model assumes a Gaussian profile for the laser beam and calculates a Maxwell−Boltzmann distribution of molecular velocities in the molecular beam

$$\frac{N_\upsilon}{N} = 4\pi\left(\frac{m}{2\pi kT}\right)^{3/2}\upsilon^2\exp(-m\upsilon^2/2kT) \quad (3)$$

where N_υ/N is the number density at velocity (υ), *m* is the mass of the radical, *k* is Boltzmann's constant, and *T* is the translational beam temperature (Θ_T) in kelvin. The length of time a molecule has to travel along the molecular beam axis is experimentally determined by the time required to trigger and fire the laser, the gate delay, and the gate width.[18] The simulation generates a spatial distribution similar to the one-dimensional cross-sectional representation of the ICCD image data. The simulated curve that best represents the experimental data gives Θ_T for the molecule of interest as determined by a nonlinear least-squares regression analysis. Values obtained from the velocity simulation are used in the reactivity simulation to model IRIS data.

III. Results

A. Spectroscopy. The spectral selectivity of the LIF technique allows identification and independent study of one specific radical in a molecular beam populated with many different species. Figure 2 shows an experimental fluorescence excitation spectrum for OH in a molecular beam formed from a 20:80 TEOS/O_2 plasma ($P = 85$ W) and the calculated line positions for the $A^2\Sigma^+ \leftarrow X^2\Pi$ (0,0) transition of OH using the molecular constants of Coxon.[29] The excellent agreement between the calculated line positions and experimental fluorescence peaks shows the fluorescing species is indeed OH. The rotational temperature (Θ_R) of the molecular beam is estimated by comparing the peak intensities of different rotational state bands in the experimental fluorescence excitation spectrum to peak intensities from spectra calculated at different Θ_R. We

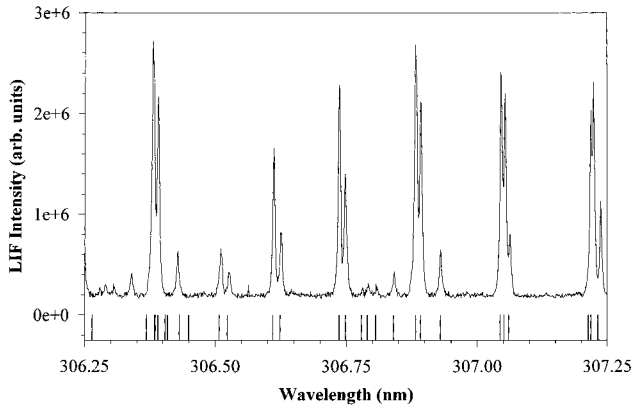

Figure 2. Experimental fluorescence excitation spectrum of OH in a 20:80 TEOS/O_2 (P = 85 W) molecular beam. Plotted below the experimental spectrum are line positions calculated using the molecular constants of Coxon.[29]

determined $\Theta_R = 440 \pm 50$ K for OH in a molecular beam formed from a 20:80 TEOS/O_2 plasma (P = 85 W).

The IRIS method for measuring radical reactivities is based on normalizing the signal from scattered radicals to the signal from radicals in the incident molecular beam. Measuring LIF signals in the molecular beam as a function of laser pulse energy (3×10^{-6}–9×10^{-4} J) shows a typical saturation curve with rapid signal increase up to 1×10^{-4} J followed by a more gradual rise at higher energies. All data are obtained with laser pulse energies of 4×10^{-4}–2×10^{-3} J, clearly in the saturated regime. Thus, our measurements are not adversely affected by small fluctuations in laser power.

B. Spatial Dependence. We have previously reported the reactivity of the OH radical in a 20:80 TEOS/O_2 plasma (P = 85 W) as 0.40 ± 0.10 while depositing SiO_2 on a 300 K silicon substrate.[19] This reactivity value was obtained using the numerical simulation without Doppler or rotational state effects included. Figure 3 shows the two-dimensional ICCD images for OH under the same conditions. LIF from OH radicals in the incident molecular beam is shown in Figure 3a. In Figure 3b, the substrate has been rotated into the path of the molecular beam, and the LIF signal includes both OH radicals in the molecular beam and those scattering from the surface. Figure 3c is the difference between parts b and a, showing the OH radicals scattered from the surface. The broad spatial distribution and the shift of the scattered signal peak maximum away from the incident molecular beam signal maximum indicates the OH radicals scatter with a cosine angular distribution.

Figure 4 shows the one-dimensional cross sections corresponding to Figure 3a,c. A full simulation of the data in Figure 4, including both Doppler and rotational state effects, yields a reactivity of 0.40 ± 0.05 for OH under these conditions, in excellent agreement with our previously reported results.[19] Thus, the inclusion of Doppler and rotational state effects produces a more refined reactivity value. Averaging all of our data sets taken over a period of six months yields a recommended reactivity value for OH of 0.41 ± 0.04 at the surface of a depositing SiO_2 film.

The molecular beam formed from the plasma will deposit a thin film onto the substrate in IRIS experiments. When removed from the IRIS apparatus, the silicon substrate used for reactivity experiments with a 20:80 TEOS/O_2 (P = 85 W) plasma clearly shows a thin film on the surface with the dimensions of the molecular beam. Analysis of this film by FTIR compares well with published FTIR spectra for SiO_2 films deposited from TEOS/O_2 in our laboratories,[30] indicating that the deposited film is indeed SiO_2.

C. Velocity Distributions. As described above in section IIB.2, the velocity of OH in a 20:80 TEOS/O_2 plasma molecular beam is measured by two methods. Figure 5 shows a one-dimensional plot of OH LIF signal intensity as a function of gate delay from 1.252 to 3.252 μs using a 20:80 TEOS/O_2 plasma (P = 85 W). As gate delay time is increased, the position of the LIF intensity peak maxima clearly shifts, the peak width increases, and the intensity of the fluorescence decreases. Measurement of the distance the peak maximum moves gives $\Theta_T = 880 \pm 270$ K. The large error limits are a result of the relatively coarse measurement method. At longer gate delays, fluorescence intensities are below our detection limit. This is primarily due to the limited fluorescence lifetime of OH.

Figure 5 also shows the simulated LIF intensity profiles generated by the velocity distribution model. The model accurately describes the data for gate delays ranging from 1.252

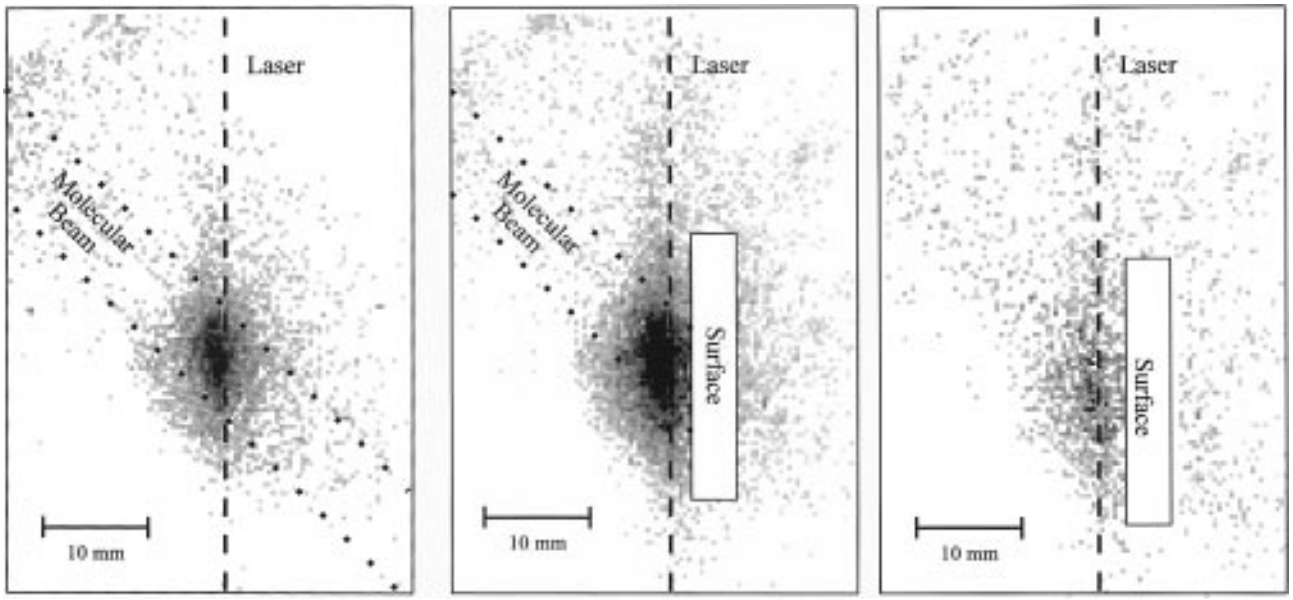

Figure 3. Spatially resolved two-dimensional ICCD images of LIF signal for the OH Q_1 (1.5) rotational state (A) in a 20:80 TEOS/O_2 (P = 85 W) molecular beam (no substrate) and (B) with a 300 K Si substrate rotated into the path of the molecular beam at a laser−surface distance of 3 mm. Image C is the difference between the images shown in (A) and (B) and shows only OH molecules scattering from the surface. LIF signals with the highest intensity appear as the darkest regions in the images. Dashed lines indicate the location of the molecular beam and the laser beam.

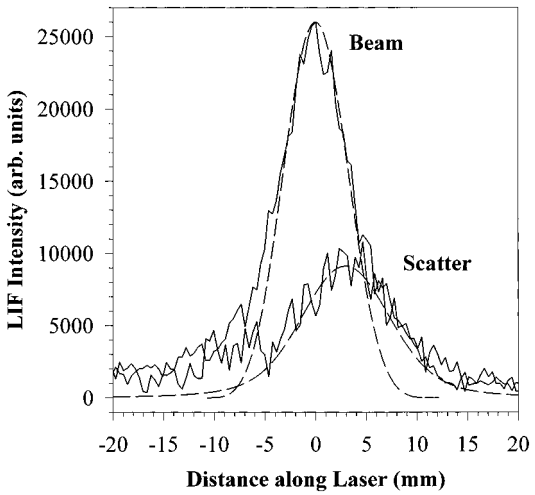

Figure 4. Comparison of cross-sectional experimental data of Figure 3 and theoretical simulations of LIF signals from OH Q_1 (1.5) rotational state in 20:80 TEOS/O_2 (P = 85 W) plasma molecular beam (no surface) and scattered from the surface (laser−surface distance of 3 mm). Dashed lines are simulated curves from the reactivity simulation described in the text, giving a value for S of 0.60 ± 0.05. This corresponds to a reactivity for OH of 0.40 ± 0.05.

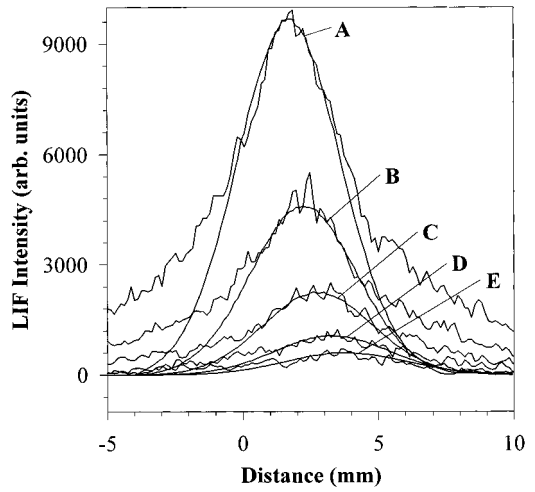

Figure 5. Velocity data for OH radicals in a molecular beam formed from a 20:80 TEOS/O_2 plasma at 85 W applied rf power. LIF intensity is plotted as a function of distance the molecules have traveled. Five ICCD gate delay times are shown: (A) 1.252, (B) 1.752, (C) 2.252, (D) 2.752, and (E) 3.252 μs. Simulated curves using the velocity model described in the text are also shown, calculated with Θ_T = 912 K.

to 3.252 μs. The average velocity is calculated using a weighted average of all five gate delay times and yields $\Theta_T = 912 \pm 20$ K for the 85 W 20:80 TEOS/O_2 plasma. We also measured the velocity of OH at a higher rf plasma power, P = 115 W, and find $\Theta_T = 1063 \pm 36$ K, significantly higher than at P = 85 W. At lower P, the OH LIF signal is weak, precluding velocity measurements at gate delay times greater than 1.752 μs. The good agreement between the simulated curves and the data in Figure 5 indicates the OH velocities in the molecular beam are well described by a Maxwell−Boltzmann distribution.

D. Substrate Temperature Dependence. To further characterize OH radicals in the molecular beam, the rotational temperature of the beam is determined. As noted above, a value of $\Theta_R = 440 \pm 50$ K is obtained from the OH fluorescence excitation spectrum. A second method to determine Θ_R involves analysis of the J-state dependence of the molecule's reactivity as a function of T_S. Figure 6 shows the experimental scattering ratio, Δ_{exp}, for three rotational states of the Q_1 branch of OH as a function of T_S. At T_S = 300 K, modeling the data yields $R = 0.40 \pm 0.05$, $R = 0.60 \pm 0.05$, and $R = 0.34 \pm 0.10$ for the J = 1.5, 2.5, and 5.5 states, respectively. As the substrate temperature is increased, these values do not describe the data accurately. Modeling the reactivity at elevated T_S results in significantly lower values for R. Also shown in Figure 6 is a numerical simulation for the scattering ratio, Δ_{cal}, assuming 85% scatter for all T_S which fit the data reasonably well at T_S > 350 K for all three J states. The substrate temperature at which the simulated curves (for R = 0.15) for all three rotational states intersect yields an estimate of Θ_R for OH in the molecular beam. From Figure 6, we estimate $\Theta_R = 450 \pm 20$ K, in excellent agreement with Θ_R obtained from the fluorescence excitation spectrum. The agreement in reactivity values obtained for the three J states indicates there is no rotational state dependence to the OH reactivity.

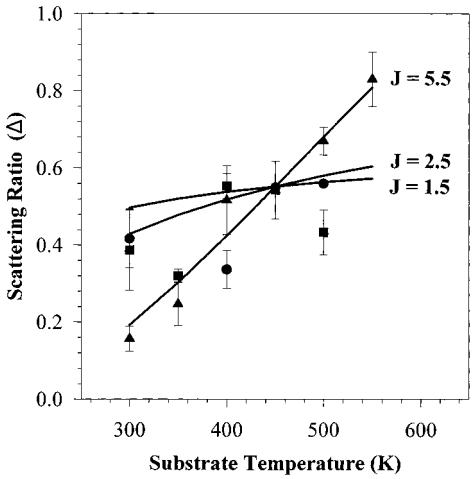

Figure 6. Substrate temperature dependence of the experimental scattering ratio, Δ_{exp}, on a Si substrate for the following OH rotational states: J = 1.5 (circles), 2.5 (squares), and 5.5 (triangles). Solid lines are the simulated substrate temperature dependence, assuming R = 0.15 for all substrate temperatures. The intersection of the R = 0.15 simulation lines gives the rotational temperature, $\Theta_R = 450 \pm 20$ K, for OH in a 20:80 TEOS/O_2 (P = 85 W) plasma.

E. Applied rf Power Dependence. A more complete understanding of the role of OH during deposition of SiO_2 is gained by measuring the surface reactivity as a function of different deposition parameters. As rf power increases 5-fold from 22 to 115 W, LIF signal intensity in the molecular beam also increases 5-fold (Figure 7). As the concentration or number density of a fluorescing molecule is directly proportional to the LIF intensity,[31] an increase in LIF intensity corresponds to an increase in number density of OH. We have also measured R for OH at these rf powers and do not observe a significant change in the reactivity. In independent film deposition experiments, we find that increasing P results in less OH incorporation in the film, a decrease in deposition rate, and an increase in the ambient substrate temperature.[32] IRIS experiments do not exactly duplicate these deposition conditions because the substrate is not directly in the plasma chamber. Our results indicate that these changes in film properties do not, however, significantly affect the OH reactivity measured in IRIS experiments.

F. O_2 Dependence. Increasing the amount of O_2 in the plasma may also affect the behavior of OH in SiO_2 depositions. We monitored OH LIF as the fraction of O_2 in the plasma is increased. LIF from OH radicals is not detected until O_2 in the plasma exceeds 50%. OH LIF signal intensity increases dramatically as percent O_2 is increased (Figure 8). These results show that a direct correlation exists between the O_2 concentration and the production of OH in TEOS plasmas.

To unequivocally identify the source of oxygen in the OH radical, isotopically labeled $^{18}O_2$ was used as the oxidant in the

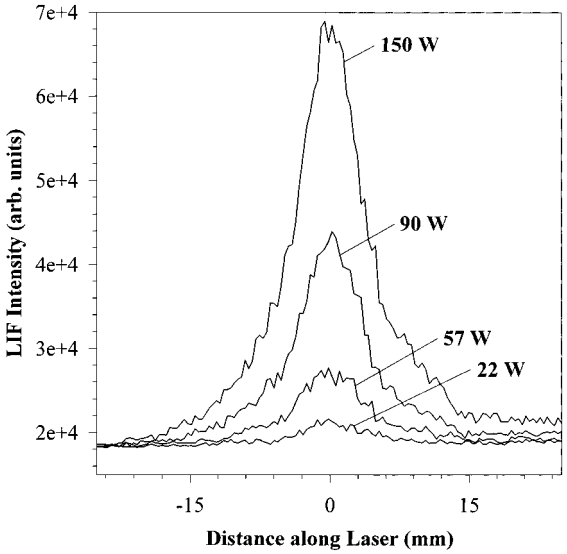

Figure 7. LIF intensity for OH in a 20:80 TEOS/O_2 plasma as a function of rf power applied to the plasma source.

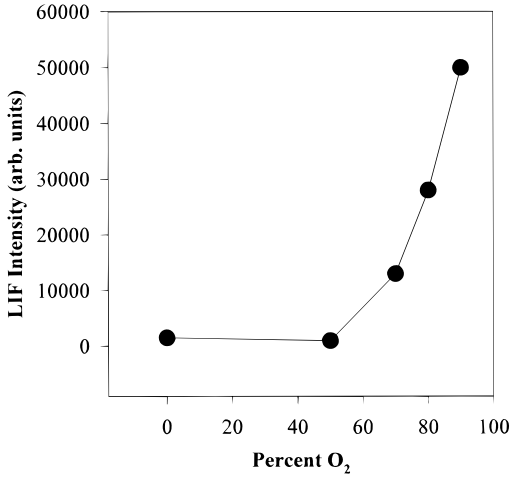

Figure 8. LIF intensity for OH in a 20:80 TEOS/O_2 (P = 85 W) plasma as a function of percent O_2 added to the gas feed.

plasma. Initially, O_2 was introduced to the plasma, and LIF signal was observed at 307.860 nm, corresponding to the ^{16}OH $Q_1(J = 1.5)$ state. While monitoring LIF signals at this wavelength, the oxygen source was switched to $^{18}O_2$. With $^{18}O_2$, we observe a significant decrease in the LIF signal at this wavelength. An intense LIF signal was detected, however, at 307.8525 nm, corresponding to ^{18}OH. There is no peak at this laser wavelength in the fluorescence excitation spectrum obtained using O_2.[33] The ^{18}OH data in Figure 9 was modeled as described above and yields $R = 0.42 \pm 0.08$, in excellent agreement with that obtained for the ^{16}OH (Figure 4). These data definitively show OH is produced by the addition of O_2 and not from the decomposition of TEOS.

IV. Discussion

Characterization of plasma components and their interactions with a substrate surface during modification is vital to understanding the underlying chemical mechanisms of plasma processing. Such characterization is difficult because plasma activation of a gas creates a multitude of potentially reactive species. Large precursor molecules such as TEOS exacerbate the problem by providing more fragmentation pathways. Even in TEOS-based systems, however, the actions of gas-phase ions and small molecules are thought to assist the deposition process by further decomposing adsorbed TEOS fragments, removing

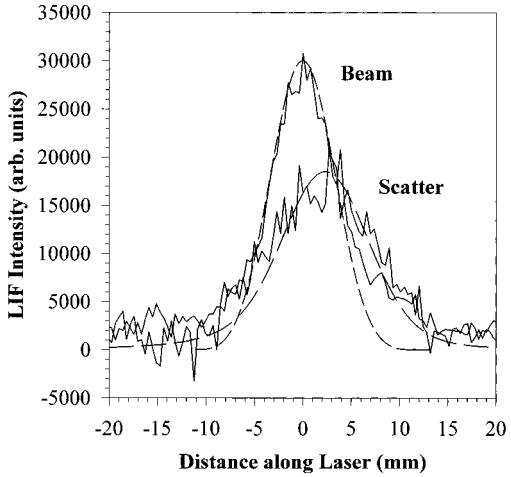

Figure 9. Cross-sectional data for LIF signals from ^{18}OH in a 20:80 TEOS/$^{18}O_2$ plasma molecular beam (no surface) and scattered from the surface (laser−surface distance of 3 mm). Data were taken at a laser wavelength of 307.8525 nm. Dashed lines are simulated curves from the reactivity simulation described in the text, giving a value for S of 0.58 ± 0.08. This corresponds to a reactivity for OH of 0.42 ± 0.08.

hydrocarbon species, and densifying the SiO_2 film.[1,8−12] Molecular level studies of the formation and reactions of small species such as OH are, therefore, important to the elucidation of process mechanisms. Here, we discuss the implications of our work on the mechanism for OH formation in the plasma, the surface reactivity of OH radicals, and the possible roles of OH in the deposition of SiO_2 from TEOS/O_2 plasmas.

A. OH Formation. The IRIS technique used here allows identification of a specific plasma species and measurement of internal and translational energies as well as surface reactivities of the radical of interest. In addition, the mechanism by which a reactive gas-phase molecule is formed can be determined. We have previously noted that, in a 100% TEOS plasma, formation of the OH radical would necessitate cleavage of both the Si−O and C−O bonds in an Si−OC_2H_5 group, cleavage of a C−H bond, and concomitant formation of an O−H bond.[19] The absence of OH radicals in a 100% TEOS plasma indicates this reaction path is unlikely. The addition of O_2 to TEOS provides another source of oxygen atoms. Plasma activation of O_2 creates oxygen atoms[1] which can then react with TEOS to produce OH radicals. More oxygen radicals are produced at higher O_2 concentrations and rf powers.[34−36] As we have shown here, the LIF signal from OH increases monotonically with O_2 concentration and with rf power, suggesting the source of O is the added oxidant. Our isotopically labeled $^{18}O_2$ studies confirm the source of oxygen in OH is indeed the added oxidant.

Further support for this H atom abstraction mechanism to form OH is gleaned from measurement of the radical's internal and translational temperatures. For P = 85 W, the translational temperature ($\Theta_T = 912 \pm 20$ K) of OH in our molecular beam is significantly higher than its rotational temperature ($\Theta_R = 450 \pm 20$ K). Θ_T increases to 1063 ± 36 K when P is increased to 115 W. This is in sharp contrast to the earlier work on OH using a 100% H_2O plasma, where it was found that Θ_T was essentially the same as Θ_R.[16] Equal internal and translational temperatures implies a long-lived HO···H decomposition intermediate allowing for equipartitioning of energy in the transition state and hence in the products.[37] This is typical for simple unimolecular bond rupture, such as formation of OH from H_2O, where the potential energy barrier is small.[37]

In the TEOS/O_2 system, however, the OH radical is formed through a bimolecular collision of an oxygen atom with a TEOS

molecule or fragment. Here, the potential barrier for reaction may be high, or there may not be a long-lived transition state.[37,38] This will reduce the amount of energy randomization in the products.[37] Reactions between $O(^3P)$ and linear or branched alkanes to form OH show the reaction involves strong interaction with only the individual C−H bonds, rather than with the entire hydrocarbon molecule.[38,39] Population of only a few rotational states of OH in these reactions suggests the reactions occur through collinear intermediates.[39] Cleavage of the R−HO bond then produces only translational or vibrational excitation.[39] Our observation of a significantly higher translational energy suggests OH is formed in the $TEOS/O_2$ system through a similar direct bimolecular reaction, abstraction of hydrogen by O atoms. This is supported by our observation that an increase in P results in a higher Θ_T for OH and a concomitant increase in OH production. This is the first time the mechanism for formation of a plasma radical from the reaction of two precursor gases has been explicitly determined using IRIS experiments.

B. Reactivity. We have previously reported that the OH radical is a component of $TEOS/O_2$ plasmas with a moderate surface reactivity ($R = 0.40 \pm 0.10$) during deposition of SiO_2 on a 300 K silicon substrate from a 20:80 $TEOS/O_2$ ($P = 85$ W) plasma.[19] This reactivity value was obtained using the reactivity model without including Doppler or rotational state effects. Here, using the full model, we confirm $R = 0.41 \pm 0.04$ for OH in this system. As discussed previously, this moderate reactivity indicates two types of surface interactions are occurring. A fraction of the incident OH molecules adsorb onto the substrate surface, thermally equilibrate, and then desorb.

$$OH(g) + * \rightleftarrows OH(ads)$$

The remaining fraction of OH radicals react at the surface, disappearing from the gas phase.

$$OH\ (ads) \rightarrow \text{products}$$

Based on the reactivity measurements made here, ~60% of the molecules desorb from the surface and ~40% react to form other products and do not return to the gas phase.

Although there are very few studies in the literature for direct comparison to our results, the OH radical has been investigated by the IRIS technique using a 100% H_2O plasma molecular beam.[14,16,20] For OH incident on a 300 K silicon nitride (Si_3N_4) substrate in this system, Buss and co-workers found $R = 0.57 \pm 0.05$.[16] We have measured a similar value for OH in this system on a 300 K Si substrate, $R = 0.55 \pm 0.10$.[14] Both of these values are significantly higher than R for OH in a 20:80 $TEOS/O_2$ plasma measured here. This difference in reactivity is most likely due to differences between surface species present on each substrate. In the H_2O:Si_3N_4(s) system, the H_2O plasma converts the nitride to oxide and hydroxylates much of the oxide surface. The OH is thought to undergo an exchange reaction with the surface silanol groups: incoming OH abstracts a hydrogen and desorbs as H_2O, and the silanol groups are regenerated by other species present in the H_2O plasma.[16] In the $TEOS/O_2$:Si(s) system, the incoming OH is exposed to many different types of surface species: di- or triethoxysilanes, silanols, hydrocarbons, silicon, silicon oxides, or hydrides.[7,9−12] The OH can react with Si sites to form silanols or can abstract hydrogen from hydrocarbon moieties and desorb as H_2O.[39] Reaction between OH and these different surface species may occur at different rates or with different probabilities. Thus, the difference in surface active sites in each plasma system may account for the observed differences in OH reactivity.

Although the magnitude of the reactivity differs greatly between the H_2O:Si_3N_4(s) and $TEOS/O_2$:Si(s) systems, the behavior of OH as a function of T_S is similar. The reactivity of OH in the $TEOS/O_2$:Si(s) system decreases from 0.41 ± 0.04 to 0.15 ± 0.05 as T_S is increased from 300 to 550 K. In the H_2O:Si_3N_4(s) system, the reactivity of OH decreases from 0.57 ± 0.05 at 300 K to 0.00 ± 0.05 for $T_S \geq 500$ K. In the latter system, this decrease in R was attributed to the loss of silanol surface coverage at high T_S and to the decrease in the activation energy for desorption relative to the activation barrier for reaction.[16] With the $TEOS/O_2$:Si(s) system, several surface active species may remain on the surface at high T_S.[10,40] Temperature-programmed desorption (TPD) studies under ultrahigh-vacuum (UHV) conditions by Tedder et al. show that dissociative TEOS adsorption on SiO_2 at substrate temperatures up to 450 K produces di- and triethoxysiloxanes on the surface.[41,42] These studies also show that both isolated and geminal surface hydroxyl groups are important in the adsorption reaction of TEOS with SiO_2.[42,43] From vibrational spectroscopy, the only species remaining on the SiO_2 surface at 800 K are a monoethoxysiloxane and a geminal hydroxyl species.[42] Similar results have been observed for TEOS decomposition on TiO_2 substrates.[40] Thus, we believe the OH radicals are reacting with these species, accounting for significant reactivity even at elevated temperatures.

The change in R as a function of T_S may indicate two types of surface reactions for OH during deposition of SiO_2 from a $TEOS/O_2$ plasma. First, OH may be reacting with the Si substrate to form a silanol group. As the substrate temperature increases, desorption of OH becomes favored, thus creating fewer SiOH groups through this reaction. Deposition studies show that as T_S increases, the concentration of SiOH groups decreases, densifying the film.[10,11,32,42] This is consistent with the observation of a decrease in R for OH at elevated T_S.

The second, more likely, reaction involves abstraction of a hydrogen atom from either a SiOH or a hydrocarbon moiety on the surface and subsequent desorption of H_2O. The effect of increasing T_S on this reaction pathway would be 2-fold. At high T_S, condensation of SiOH groups decreases the availability of this reaction partner for OH.[10,11] In the H_2O:Si_3N_4(s) system, SiOH was the only hydrogenated surface species available for reaction with OH. Thus, R decreased to essentially zero at elevated T_S. In our system, however, R only decreases to 0.15, indicating that SiOH groups are not the only reaction partner for OH. As noted above, TEOS fragments remain on the surface at elevated T_S, maintaining a source of hydrogen for abstraction by OH. It should be noted, however, that the surface coverage of these species does decrease with T_S, but does not go to zero, even at $T_S = 800$ K.[42] Thus, although the reactivity in our system decreases to 0.15, reaction of OH at the surface is not entirely eliminated.

A final point about the surface reactivity measurements for OH in the $TEOS/O_2$ system should be made. In our first account of this system, we reported an observation of a decrease in R with increasing rf power and suggested it was due to compensating reactions.[19] A more complete analysis of these data, however, shows no significant change in R as rf power is increased. This implies there are no compensating reactions occurring at the surface. Therefore, the R value reported here is believed to correspond solely to incident OH radicals and not to the production of gas-phase OH through compensating reactions.

D. Role of OH. We have identified the OH radical as a component of a $TEOS/O_2$ plasma and have measured its surface reactivity during deposition of SiO_2. Additional experiments have determined the mechanism for formation of OH in the plasma as well as its translational and internal energies.

Although the number density of OH in this plasma is small,[47] we believe it is an important component in the SiO_2 deposition scheme.

Our results demonstrate gas-phase OH is formed in the plasma through hydrogen abstraction by O atoms,

$$O(^3P)(g) + Si(OC_2H_5)_x(g) \rightarrow OH(^2\Pi)(g) + Si(OC_2H_5)_{x-1}(OC_2H_4)^{\bullet}(g)$$

where $Si(OC_2H_5)_{x-1}(OC_2H_4)^{\bullet}$ denotes any TEOS fragment. This is important because the intact TEOS molecule does not contribute significantly to the deposition process, but various TEOS fragments are considered integral to film formation.[7,9,10,41,42] Thus, the creation of OH also results in formation of important deposition precursors in the plasma.

At the substrate surface, OH also contributes to the deposition process. As noted above, gas-phase OH radicals can react with surface Si atoms to form SiOH groups. For microelectronic applications, silanols are undesirable because they disrupt the tetrahedral network and decrease the dielectric integrity of the film.[11] We believe, however, that the primary role of OH at the gas−surface interface during SiO_2 deposition is hydrogen abstraction from surface species such as SiOH and hydrocarbons. Hydrogen abstraction from either of these groups serves to improve film quality by increasing the stoichiometry of the SiO_2 film. Consequently, we have demonstrated that even diatomic molecules such as OH are integral to the complex deposition of technologically relevant materials such as SiO_2. Furthermore, the detailed information about OH in TEOS/O_2 plasmas acquired from our research, including surface reactivities, energy distributions, and the mechanism for formation, is critical to the accurate modeling of the molecular processes involved in these systems.

V. Summary

The presence of the $OH(X^2\Pi)$ radical in a 20:80 TEOS/O_2 plasma and its reactivity at the surface of a depositing SiO_2 film have been characterized using the IRIS technique. Isotopically labeled $^{18}O_2$ studies show the OH radical is formed by the direct abstraction of a hydrogen atom from TEOS fragments by oxygen atoms. This is supported by velocity distribution measurements of OH that reveal the translational temperature of OH increases with increasing rf power and is significantly higher than the rotational temperature. The reactivity of OH on a 300 K substrate is 0.41 ± 0.04 and decreases to 0.15 ± 0.05 at $T_S > 350$ K. OH is believed to play an important role in the deposition of SiO_2 films from TEOS/O_2 plasmas by producing gas-phase deposition precursors and by promoting surface silanol and hydrocarbon removal through hydrogen abstraction.

Acknowledgment. Financial support for this research comes from the National Science Foundation (CHE-951157). We also acknowledge helpful discussions with Dr. Laura L. Tedder and Prof. Peter B. Armentrout.

References and Notes

(1) Lieberman, M. A.; Lichtenberg, A. J. *Principles of Plasma Discharges and Materials Processing*; John Wiley and Sons: New York, 1994.

(2) Jansen, F. In *Plasma Deposited Thin Films*; Mort, J., Jansen, F., Ed.; Chemical Rubber: Boca Raton, FL, 1986.

(3) Maeda, K.; Fisher, S. M. *Solid State Technol.* **1993**, *36*, 83.

(4) Hills, G. W.; Harrus, A. S.; Thoma, M. J. *Solid State Technol.* **1990**, *33*, 127.

(5) Raupp, G. B; Levedakis, D. A.; Cale, T. S. *J. Vac. Sci. Technol. A* **1995**, *13*, 676.

(6) Stout, P. J.; Kushner, M. J. *J. Vac. Sci. Technol. A* **1993**, *11*, 2562.

(7) Chang, C.-P.; Pai, C. S.; Hsieh, J. J. *J. Appl. Phys.* **1990**, *67*, 2119.

(8) Tochitani, G.; Shimozuma, M.; Tagashira, H. *J. Vac. Sci. Technol. A* **1993**, *11*, 400.

(9) Pai, C. S.; Chang, C.-P. *J. Appl. Phys.* **1990**, *68*, 793.

(10) Deshmukh, S. C.; Aydil, E. S. *J. Vac. Sci. Technol. B* **1996**, *14*, 738. Deshmukh, S. C.; Aydil, E. S. *J. Vac. Sci. Technol. A* **1995**, *13*, 2355. Deshmukh, S. C.; Aydil, E. S. *Appl. Phys. Lett.* **1994**, *65*, 3185.

(11) Selamoglu, N.; Mucha, J. A.; Ibbotson, D. E.; Flamm, D. L. *J. Vac. Sci. Technol. B* **1989**, *7*, 1345.

(12) Fracassi, F.; d'Agostino, R.; Favia, P. *J. Electrochem. Soc.* **1992**, *139*, 2636.

(13) Nishi, Y.; Funai, T.; Izawa, H.; Fujimoto, T.; Morimoto, H.; Ishii, M. *Jpn. J. Appl. Phys.* **1992**, *31*, 4570.

(14) McCurdy, P. R.; Bogart, K. H. A.; Dalleska, N. F.; Fisher, E. R. *Rev. Sci. Instrum.* **1997**, *68*, 1684.

(15) Ho, P.; Breiland, W. G.; Buss, R. J. *J. Chem. Phys.* **1989**, *91*, 2627.

(16) Fisher, E. R.; Ho, P.; Breiland, W. G.; Buss, R. J. *J. Phys. Chem.* **1993**, *97*, 10287.

(17) Fisher, E. R.; Ho, P.; Breiland, W. G.; Buss, R. J. *J. Phys. Chem.* **1992**, *96*, 9855.

(18) McCurdy, P. R.; Venturo, V. A.; Fisher, E. R. *Chem. Phys. Lett.* **1997**, *274*, 120.

(19) Bogart, K. H. A.; Cushing, J. P.; Fisher, E. R. *Chem. Phys. Lett.* **1997**, *267*, 377.

(20) Buss, R. J.; Ho, P. *IEEE Trans. Plasma Sci.* **1996**, *24*, 79.

(21) Buss, R. J.; Ho, P.; Weber, M. E. *Plasma Chem. Plasma Process.* **1993**, *13*, 61.

(22) Cessou, A.; Stepowski, D. *Combust. Sci. Technol.* **1996**, *118*, 361. Allan, M. G.; McManus, K. R.; Sonnefroh, D. M.; Paul, P. H. *Appl. Opt.* **1995**, *34*, 6287.

(23) Tully, F. P.; Droege, A. T.; Koszykowski, M. L.; Melius, C. F. *J. Phys. Chem.* **1986**, *90*, 691. Tully, F. P.; Goldsmith, J. E. M. *Chem. Phys. Lett.* **1985**, *116*, 345.

(24) Brauers, T.; Aschmutat, U.; Brandenburger, U.; Dorn, H.-P.; Hausmann, M.; Hessling, M.; Hofzumahaus, A.; Holland, F.; Plass-Dülmer, C.; Ehhalt, D. H. *Geophys. Res. Lett.* **1996**, *23*, 2545.

(25) This delay time accounts for the time required for the laser to trigger and fire, experimentally determined as 1.1 μs. Thus, a 1.3 μs gate delay corresponds to a 0.2 μs delay between excitation and collection of fluorescence by the ICCD.

(26) German, K. R. *J. Chem. Phys.* **1975**, *62*, 2584.

(27) Atkins, P. W. *Physical Chemistry*, 4th ed; W. H. Freeman and Company: New York, 1990.

(28) Steinfeld, J. I. *Molecules and Radiation*; MIT: Cambridge, MA, 1985.

(29) Coxon, J. A. *Can. J. Phys.* **1980**, *58*, 933.

(30) Bogart, K. H. A.; Dalleska, N. F.; Bogart, G. R.; Fisher, E. R. *J. Vac. Sci. Technol. A* **1995**, *13*, 476.

(31) Clyne, M. A. A.; McDermid, I. S. *Dynamics of the Excited State*; Lawley, K. P., Ed.; John Wiley and Sons: New York, 1982.

(32) Bogart, K. H. A; Ramirez, S. K.; Campuzano, L. A.; Bogart, G. R.; Fisher, E. R. *J. Vac. Sci. Technol. A*, to be submitted.

(33) A full excitation spectrum for OH (from 307.0 to 309.0 nm) is published in ref 19

(34) Walkup, R. E.; Saenger, K. L.; Selwyn, G. S. *J. Chem. Phys.* **1986**, *84*, 2668.

(35) Selwyn, G. S. *J. Appl. Phys.* **1986**, *60*, 2771.

(36) Collart, E. H.; Baggerman, J. A. G.; Visser, R. J. *J. Appl. Phys.* **1995**, *78*, 47.

(37) Levine, R. D.; Bernstein, R. B. *Molecular Reaction Dynamics and Chemical Reactivity*; Oxford University Press: New York, 1987; pp 426−428.

(38) Park, C . R.; Wiesenfeld, J. R. *J. Chem. Phys.* **1991**, *95*, 8166.

(39) Andresen, P.; Luntz, A. C. *J. Chem. Phys.* **1980**, *72*, 5842. Luntz, A. C.; Andresen, P. *J. Chem. Phys.* **1980**, *72*, 5851. Luntz, A. C. *J. Chem. Phys.* **1980**, *73*, 1143.

(40) Jurgens, T. A.; Rogers, J. W., Jr. *J. Phys. Chem.* **1995**, *99*, 731.

(41) Tedder, L. L.; Lu, G.; Crowell, J. E. *J. Appl. Phys.* **1991**, *69*, 7037.

(42) Tedder, L. L.; Crowell, J. E.; Logan, M. A. *J. Vac. Sci. Technol. A* **1991**, *9*, 1002.

(43) Crowell, J. E.; Tedder, L. L.; Cho, H.-C.; Cascarano, F. M.; Logan, M. A. *J. Vac. Sci. Technol. A* **1990**, *8*, 1864.

(44) We estimate the detection limit for OH in our system to be 10^9 molecules cm^{-3}. A more complete discussion of this value is given in ref 19.